Rhombohedral Shape of Hematite Nanocrystals Synthesized via Thermolysis of an Additive-free Ferric Chloride Solution

ARTICLE *in* THE JOURNAL OF PHYSICAL CHEMISTRY C · OCTOBER 2007

Impact Factor: 4.77 · DOI: 10.1021/jp075381i

Rhombohedral Shape of Hematite Nanocrystals Synthesized via Thermolysis of an Additive-free Ferric Chloride Solution

Raúl D. Rodriguez,[†] Dominique Demaille,[†] Emmanuelle Lacaze,*[,†] Jacques Jupille,[†] Corinne Chaneac,[‡] and Jean-Pierre Jolivet[‡]

Institut des NanoSciences de Paris (INSP), CNRS UMR-7588, Université Pierre et Marie Curie—Paris 6, Campus Boucicaut, 140 rue de Lourmel, 75015 Paris, France, and Chimie de la Matière Condensée de Paris, CNRS UMR-7574, Université Pierre et Marie Curie—Paris 6, 4 place Jussieu, 75252 Paris Cedex 05, France

Received: July 10, 2007; In Final Form: September 5, 2007

The morphology and structure of hematite nanoparticles synthesized from the widespread technique developed by Matijevic 30 years ago is revisited. The thermolysis of acidic ferric chloride is shown to lead to monodispersed hematite nanocrystallites of rhombohedral shape with facets belonging to the {104} family, as derived from a joint atomic force microscopy (AFM) and transmission electron microscopy (TEM) investigation. All TEM and AFM data are shown to be accurately accounted for by a unique rhombohedral model particle.

1. Introduction

Nanometrical-sized particles are today largely used for various purposes because of the huge surface area (interesting for catalysis and adsorption phenomena) and because of their specific properties dependent on their size and shape (for instance, grain boundary effects on mechanical properties, quantum size effects on electrical and optical properties, relaxation and surface phenomena on magnetic properties).[1] These effects give rise to interesting technological applications which need, however, dimensionally and morphologically well-defined particles, the more often free from aggregation. Monodispersed hematite α-Fe_2O_3 nanoparticles (HNP) have been largely used,[1−8] and the synthesis of α-Fe_2O_3 particles of various shapes (platelet, sphere, pseudocube, spindle, double ellipsoid, ...) is largely documented.[9−21] The morphology can be controlled by various factors (ferric ions concentration, acidity, nature of the anions, ...), but the particles are generally micronic in size and often polycrystalline. By thermolysis of $FeCl_3$ in acidic medium, nanometrical particles forming stable sols are obtained. Different shapes were identified, namely, cubes, hexagonal platelets, rhombohedra, and spheroids.[2,6,21−24] Cornell and Schwertmann explicitly reported that "in the absence of additives, hexagonal plates which are often rounded and rhombohedra predominate".[10]

In fact, the particle shape is more often determined from transmission electron microscopy (TEM) or atomic force microscopy (AFM), which gives rise to ambiguities because of the drawbacks inherent to these techniques. TEM shows projections of the particles along the optical axis of the microscope. Therefore, TEM micrographs and diffraction patterns must be carefully examined and compared to unambiguously determine particle shapes. Studies performed by AFM on nanoparticles underline the difficulties to accurately determine the shape and size of the particles,[25] especially if they are aggregated.[26,27] The present paper aims to combine tapping mode atomic force microscopy (TMAFM) and high-resolution transmission electron microscopy (HRTEM) to revisit the analysis of the shape of HNPs prepared by thermolysis of acidic ferric chloride in the absence of any additive. A particular goal was also to prepare well-isolated particles to obtain accurate information from AFM imaging.

2. Experimental Section

Hematite nanoparticles were synthesized by forced hydrolysis of an acidic ferric chloride solution (final pH = 2.0) at 95 °C as described by Jolivet et al.[28] for ferric nitrate solutions. A stock solution of iron(III) precursor was obtained by mixing 10 cm^3 of $FeCl_3$ (3 mol·dm^{-3} in solution 45% Riedel-de Haën) and 60 cm^3 of HCl (0.2 mol·dm^{-3}). All preparations were made using double-deionized water, filtered with a 30 000 Da membrane. An amount of 7 cm^3 of this stock solution was rapidly added under vigorous agitation into 300 cm^3 of a hot NaOH solution (10^{-2} mol·dm^{-3} obtained from NaOH aqueous solution 0.1 N Normadose, VWR) in order to obtain a pH of 2.0. NaOH solution is added drop by drop using an automatic cylinder driven by a Metrohm Combi Titerur 3D until the programmed pH value was obtained.

The final iron(III) concentration of the suspension is 10^{-3} mol·dm^{-3} for which a brown precipitate is immediately observed. The mixture was then poured in a polypropylene bottle and aged at 95 °C for 7 days without stirring. After aging, a stable colloidal suspension of red color was obtained containing the HNPs that are studied herein. An equivalent preparation procedure to the one described above is reported by Kan et al.[21] where a more detailed description is presented.

Standard X-ray diffraction (XRD) measurements were carried out with Cu Kα radiation. The crystallinity and purity of dried samples agglutinated on a glass plate were verified by XRD patterns. The observed peaks all corresponded to the expected ones for the hematite structure.[29]

The AFM (Nanoscope Dimension 3100, Veeco Instruments) was operated in tapping mode.[30] The substrate most appropriate for AFM examination of the hematite particles appeared to be MoS_2: it is very flat and can be easily renewed by cleavage.

* Corresponding author. E-mail: Emmanuelle.Lacaze@insp.jussieu.fr Phone: (+33) 1-44-27-46-54. Fax: (+33) 1-43-54-28-78.
[†] Institut des NanoSciences de Paris.
[‡] Chimie de la Matière Condensée de Paris.

10.1021/jp075381i CCC: $37.00
Published on Web 10/24/2007

For the sample preparation corresponding to AFM measurements, a 10% concentration of the aged solution was obtained by diluting in water. A drop of the diluted solution was placed in contact with a freshly cleaved MoS_2 substrate and then rapidly removed with filter paper. Well-dispersed hematite particles were obtained in this way. Without any further treatment the sample was placed for the AFM measurements that were carried on in ambient conditions.

The TEM analysis of the particles was achieved by using a JEOL 2100 field emission transmission electron microscope operated at 200 kV with a 0.18 nm resolution. Samples were prepared by depositing a drop of the diluted solution containing the α-Fe_2O_3 nanoparticles on carbon-coated copper grids. Any excess was removed with absorbent paper.

3. Results and Discussion

Monodispersed Nanoparticles. The technique of the deposition of particles by means of a drop of diluted solution on cleaved MoS_2 was perfectly successful regarding the goal of the experiment. A good dispersion of the particles on the disulfide substrate was achieved. On AFM images, hematite particles appear as isolated objects scattered over the surface (Figure 1a). A careful examination shows that all top facets reproducibly display a rhombus shape (Figure 1, parts b and c). The value of 107° of the obtuse angle is derived from the analysis of 50 HNPs giving a precision of ±2°. Particles are quite monodispersed. Their average height measured with respect to the MoS_2 substrate is 38 nm (with a precision of ±4 nm; measurement set over 50 particles). Three parts are observed on cross sections oriented parallel to the particle sides (Figure 1d) which only allows us to estimate the lateral size of the particles to be between 35 and 45 nm, of the same order of magnitude as the height. Such a height value appears consistent with the sizes previously indicated by Jolivet et al.[28] for a pH value of 2.0. The flat top reflects the low roughness of the MoS_2 surface and the flatness of the top facet. This is repeatedly observed for every particle which implies that the opposite faces, top and bottom, are systematically parallel. Asymmetry in the two lateral segments also appears systematically in all the AFM data; as for Figure 1d, it is found different angles for the left and right segments of the cross section: 64.64° and 79.47° (mean values of a set of measurements over 50 particles: 65° ± 2° and 77° ± 4°). This geometry is even visible in the topography images (Figure 1c). This point will be discussed later.

Model Rhombohedra with {104} Faces. For HRTEM analysis, the crystallites of the same solution as for AFM studies were deposited on a rough surface, the carbon-coated grids. It is worth noting that while in AFM measurements the particles were isolated over the MoS_2 substrate it was not the case for TEM measurements. Even though excess of the deposited solution drop was dried from the TEM grid by using absorbent paper, the traces left behind were large because of the low hydrophobicity of the grid as compared to the same drop on the MoS_2 which is much more hydrophobic. Another factor contributing to this difference is the significant roughness of the TEM grid as compared to the atomically flat MoS_2 substrate used in AFM. The grid roughness also leads to random orientations of the HNP as shown in the Figure 2a. Such a variety in the HNP aspect can have led in the past to misinterpretations concerning the HNP shape.

One particular TEM micrograph appears particularly interesting because it has the rhombus morphology observed by AFM (Figure 2b). The height of this particle cannot be obtained, but its lateral size is measured to be 36.86 ± 0.18 nm, in agreement with AFM measurements. Its side facets seem parallel to the crystal planes (104) and (0−14), as indexed from its power spectrum in Figure 2c. For all the particles similarly orientated, it is noted that a slight tilt allows the side faces to appear. That confirms that these faces are actually parallel to the optical axis of the microscope and coincide accurately with the (104) and

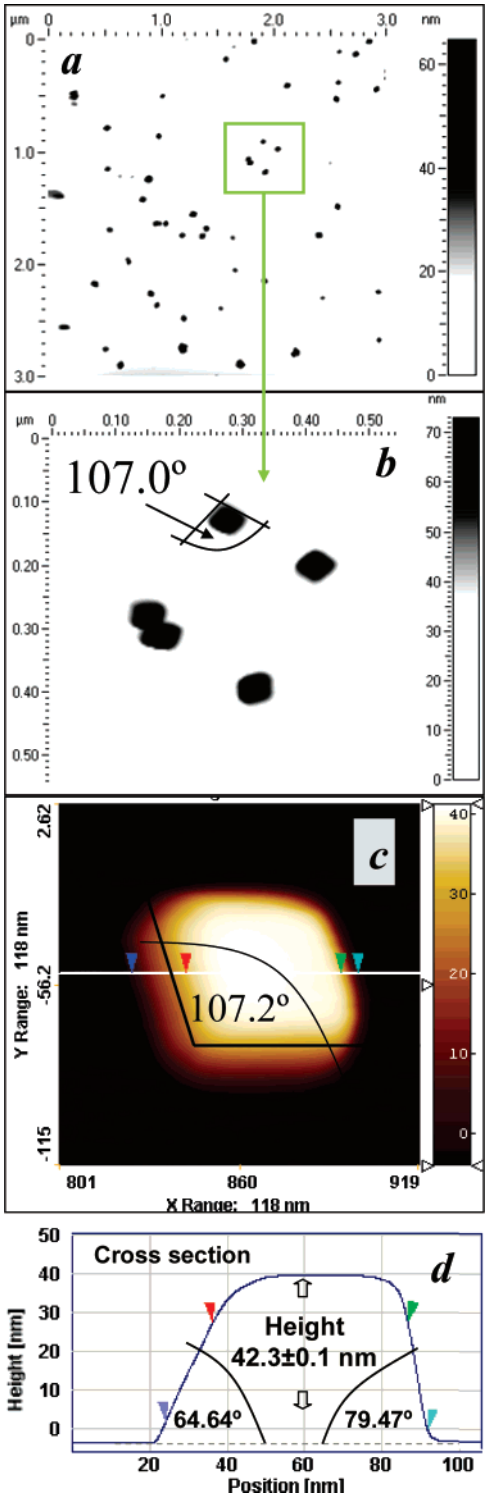

Figure 1. AFM imaging of HNP: (a) well-dispersed particles (3000 nm^2); (b) zoom on region marked in (a) where sharp rhombi are visible (550 × 550 nm^2); (c) image of a particle (118 nm^2); (d) cross profile of the particle marked in (c) showing the accurate height determination, 42.3 nm, the flatness of the top, and the dissymmetry between side's slopes, 64.64° and 79.47°. Colored arrows (for reference) in (d) correspond to those in (c).

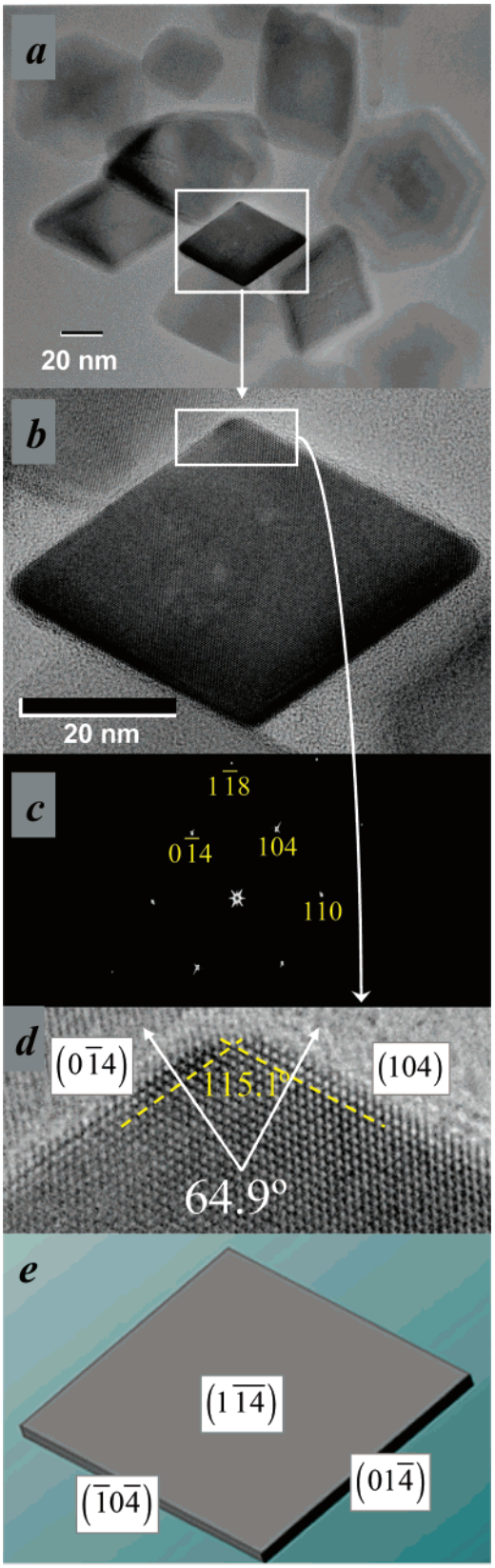

Figure 2. HRTEM images of HNP: (a) collection of particles; (b) high-resolution image of a particle displaying rhombus geometry; (c) power spectrum of image b which serves to identify the crystal facets, zone axis [−441]; (d) zoom on image b; white arrows indicates the normal vectors to the facets; (e) proposed indexation and geometry for the HNP as delimited by {104} facets.

(0−14) crystal planes (Figure 2d). Under the assumption that the α-Fe_2O_3 particles are in the shape of rhombohedra, the faces parallel to the (104) and (0−14) can be, respectively, indexed as (−10−4) and (01−4) planes. An immediate assignment of the last end faces would have implied a tilt of about 65° of the crystal shown in Figure 2b in order to put in diffraction position the crystal planes corresponding to its still unknown top and bottom facets. It was not possible because the high-resolution objective lens of our JEOL 2100 microscope allowed a 17° maximum tilt angle. However, from the observation of a large amount of hematite nanocrystals, we notice that no plane other than the {104} type ever coincided with an end facet. This led us to consider that the last two facets could also be of the {104} type and to build the model HNP shown in Figure 2e, a rhombohedral crystal with {104} type faces.

TEM and AFM Evidence for a Unique Rhombohedral Shape for α-Fe_2O_3 Nanoparticles. To check this model, it is attempted to reproduce the shapes characteristic of the hematite crystals observed on the many TEM images of α-Fe_2O_3 particles which were registered. All TEM micrographs show collections of single crystals of about similar size (Figure 2a). It would be difficult to determine their shape by rotating the sample holder because of the above-mentioned limitation in the tilt angle. It is found more appropriate to use a set of TEM micrographs of several crystals which exhibit planes perfectly orientated in Bragg position, as those presented in Figure 3. For each micrograph, a power spectrum is calculated on which the diffraction spots are indexed to identify the zone axis. Hematite crystallizes in the rhombohedral system with the $R\bar{3}c$ space group. Nevertheless, all the indexations are given in the hexagonal system as is commonly done for easiness. With this purpose, the nanocrystal shown in Figure 2b oriented along the [−441] zone axis is considered together with three other nanocrystals (Figure 3a−c) whose zone axes are identified from their power spectrum as being [−221], [−111], and [001] (Figure 3d−f). All these zone axes belong to the same plane (110) and make an angle with the [−441] axis of, respectively, 16.75°, 36.11°, and 68.47°. Therefore, this micrographs set allows us to follow the crystal shape evolution as if the [−441] axis was rotated in the (110) plane and was compared with the model oriented along these directions (Figure 3g−i). The agreement is good. It is worth noting that the hematite particle imaged in Figure 3b can be interpreted as a cube,[31] whereas that in Figure 3c could be considered as a prism with a hexagonal base.[32] In fact, the model indicates that the crystals in Figure 3, parts b and c, are rhombohedral particles viewed, respectively, along the [−111] axis and the ternary axis [001].

More evidence about this rhombohedral shape was brought by AFM analysis which was used to check the accuracy of the model of HNP. For AFM imaging, the crystals were deposed with a given face in flat contact with the substrate. Considering our crystallographic model, let us say that this is the (1−1−4) plane (Figure 4a). Then the edges delimiting the top face (−114) are the [841] and [−4−81] axes with a calculated angle of 107.3°. The value measured by AFM, 107° ± 2°, agrees perfectly as can also be seen from Figure 1c. One must not confuse with the inner angle (115.1°) between the (104) and (0−14) faces measured in Figure 2d by TEM. The angle usually given between two planes by crystallographic software is in fact the angle between the normals to these planes as illustrated by white arrows on Figure 2d.

On an AFM cross section along the short diagonal of the particle as shown in Figure 4, parts a and b, the third segment (Figure 4c) is parallel to a [−441] axis type. The complementary to the angle calculated between this axis and the normal to the bottom facet (−114) is 59.8°, close to the value of 61° ± 2°

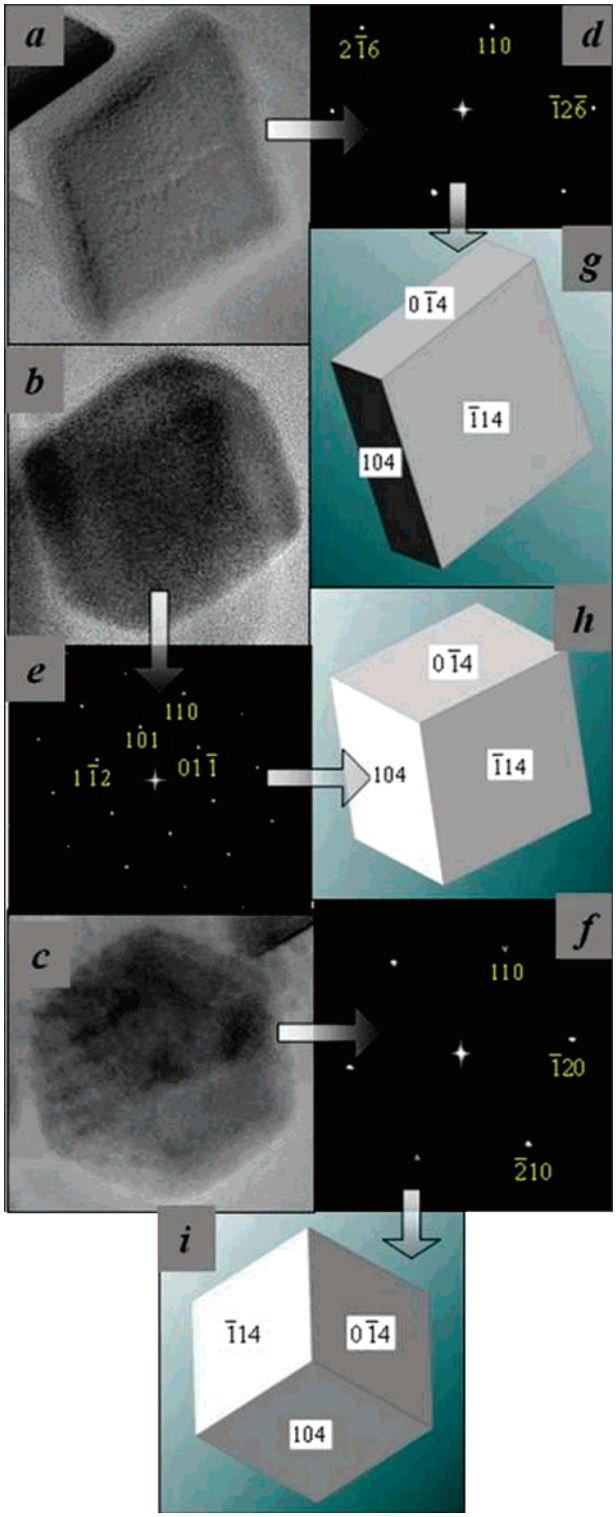

Figure 4. (a) Hypothesized HNP as measured by AFM; top view. Arrows indicate the edges corresponding to the shown crystallographic directions; (b) experimental AFM image; (c) cross profile of image in (b). Roman italic numbers I−II indicate the orientation of cross sections.

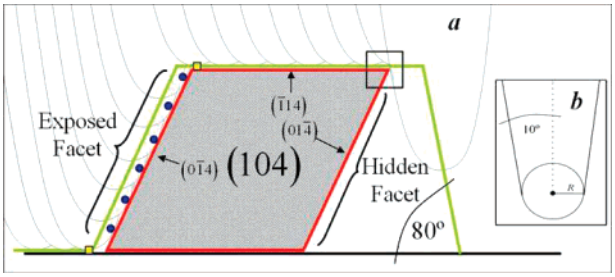

Figure 5. (a) Illustration of the tip scanning over the particle. At the left side, the same part of the tip touches the exposed side of the HNP, whereas at the right side it is the border of the particle which makes contact with the tip's side; a profile of the tip is obtained including its angle (complementary angle); (b) scheme of the tip as drawn from the nominal data.

Figure 3. (a−c) HRTEM showing the evolution of the apparent particle shape for the orientations [−221], [−111], and [001], respectively; (d−f) corresponding power spectra; (g−i) HNP model oriented along the [−221], [−111], and [001] axes.

measured by AFM (average of measurements done over 27 particles). On the AFM cross section of the Figure 1d, the angle between the substrate and the third segment is not calculated so easily. The plane containing this cross section does not correspond to a crystallographic plane, and the third segment does not coincide with a crystallographic axis. However, an approximate calculus[33] gives a value of 63.9° which is consistent with the 65° ± 2° measured by AFM. The general agreement between the angles calculated from the crystallographic model and those measured by AFM confirms unambiguously that all the HNP facets belong to the {104} family.

The HNP model also explains the asymmetry observed on AFM cross sections as schematized in Figure 5a. Contrary to the exposed facets for which only one point of the tip interacts with the whole facet, hidden facets are not accessible to the AFM tip. The border between the hidden facet and the top facet (square in Figure 5a) interacts with every point of the AFM tip, finally leading to a profile of the tip instead of a profile of the HNP itself. The green line shown in Figure 5a is an emulation of the pathway followed by the tip when scanning a model HNP, with a tip geometry drawn from the nominal data given by the manufacturer (half-cone angle 10° and tip radius 10 nm—Figure 5b). It shows that the angle measured on the side of the hidden facet directly corresponds to the complementary value of the tip half-cone angle. The values obtained in Figures 1d (10.53°) and 4c (10°) are in good agreement with the manufacturer specification. The relatively big dispersion obtained (±4°) is explained as due to the variations in tip aspect ratio and shape anisotropy. Our results consequently open the possibility to use these HNP as tip characterizers.

4. Conclusions

The shape and structure of the crystalline hematite α-Fe_2O_3 nanoparticles prepared by forced hydrolysis of acidic ferric chloride in the absence of any additives has been revisited. By a combined TEM and AFM study, it is evidenced that, in such conditions, the hematite particles are monodispersed and all show a unique rhombohedral shape with {104} facets.

The {104} morphology of particles seems to result from energetic and structural origin. This point is now an open question and will be discussed elsewhere.

References and Notes

(1) Bødker, F.; Mørup, S. Size dependence of the properties of hematite nanoparticles. *Europhys. Lett.* **2000**, *52* (2), 217.

(2) Raming, T. P.; Winnubst, A. J. A.; van Kats, C. M.; Philipse, A. P. The synthesis and magnetic properties of nanosized hematite (α-Fe_2O_3) particles. *J. Colloid Interface Sci.* **2002**, *249*, 346.

(3) Wang, Y.; Muramatsu, A.; Sugimoto, T. FTIR analysis of well-defined α-Fe_2O_3 particles. *Colloids Surf., A* **1998**, *134*, 281.

(4) He, Y. P.; Miao, Y. M.; Li, C. R.; Wang, S. Q; Cao, L.; Xie, S. S.; Yang, G. Z.; Zou, B. S.; Burda, C. Size and structure effect on optical transitions of iron oxide nanocrystals. *Phys. Rev. B* **2005**, *71*, 125411.

(5) Wang, J.; White, W. B.; Adair, J. H. Near-infrared luminescence of ferric oxide particles. *Mater. Lett.* **2006**, *60*, 2013.

(6) Delgado, A. V.; González-Caballero, F. Inorganic particles as colloidal models. Effects of size and shape on the electrokinetics of hematite α-Fe_2O_3. *Croat. Chem. Acta* **1998**, *71* (4), 1087.

(7) Frandsen, C.; Bahl, C. R. H.; Lebech, B.; Lefmann, K.; Theil Kuhn, L.; Keller, L.; Andersen, N. H.; Zimmermann, M. v.; Johnson, E.; Klausen, S. N.; Mørup, S. Oriented attachment and exchange coupling of α-Fe_2O_3 nanoparticles. *Phys. Rev. B* **2005**, *72*, 214406.

(8) Wu, C.; Yin, P.; Zhu, X.; OuYang, C.; Xie, Y. Synthesis of hematite (α-Fe_2O_3) nanorods, diameter size and shape effects on their applications in magnetism, lithium ion battery, and gas sensors. *J. Phys. Chem. B* **2006**, *110*, 17806.

(9) Matijevic, E.; Scheiner, P. *J. Colloid Interface Sci*. **1978**, *63*, 509.

(10) Cornell, R. M.; Schwertmann, U. *The Iron Oxides*; Wiley-VCH: Weinheim, Germany, 2003; p 82.

(11) Hamada, S.; Matijevic, E. *J. Chem. Soc., Faraday Trans. 1*. **1982**, *78*, 2147.

(12) Ozaki, M.; Kratohvil, S.; Matijevic, E. *J. Colloid Interface Sci.* **1984**, *102*, 146.

(13) Ishikawa, T.; Matijevic, E. *Langmuir* **1988**, *4*, 26.

(14) Morales, M. P.; Gonzalez-Carreno, T.; Serna, C. J. *J. Mater. Res.* **1992**, *7*, 2538.

(15) Bailey, J. K.; Brinker, C. J.; Mecartney, M. L. *J. Colloid Interface Sci.* **1993**, *157*, 1.

(16) Sugimoto, T.; Sakata, K.; Muramatsu, A. *J. Colloid Interface Sci.* **1993**, *159*, 372.

(17) Ocana, M.; Morales, M. P.; Serna, C. J. *J. Colloid Interface Sci.* **1995**, *171*, 85.

(18) Ocana, M.; Rodriguez-Clemente, R.; Serna, C. J. *Adv. Mater.* **1995**, *7*, 212.

(19) Sugimoto, T.; Muramatsu, A. *J. Colloid Interface Sci.* **1996**, *184*, 626.

(20) Sugimoto, T.; Wang, Y.; Itoh, H.; Muramatsu, A. *Colloids Surf., A* **1998**, *134*, 265.

(21) Kan, S.; Yu, S.; Peng, X.; Zhang, X.; Li, D.; Xiao, L.; Zou, G.; Li, T. Formation process of nanometer-sized cubic ferric oxide single crystals. *J. Colloid Interface Sci.* **1996**, *178*, 673.

(22) Reeves, N.; Mann, S. Influence of inorganic and organic additives on the tailored synthesis of iron oxides. *J. Chem. Soc., Faraday Trans.* **1991**, *87* (24), 3875.

(23) Jones, F.; Ogden, M. I.; Oliveira, A.; Parkinson, G. M.; Richmond, R. W. The effect of phosphonate-based growth modifiers on the morphology of hematite nanoparticles formed via acid hydrolysis of ferric chloride solutions. *Cryst. Eng. Commun.* **2003**, *5* (30), 159.

(24) Gee, S. H.; Hong, Y. K.; Sur, J. C.; Erickson, D. W.; Park, M. H.; Jeffers, F. Spin orientation of hematite (α-Fe_2O_3) nanoparticles during the Morin transition. *IEEE Trans. Magn.* **2004**, *40* (4), 2691.

(25) Maurice, P. A. Review: Applications of atomic-force microscopy in environmental colloid and surface chemistry. *Colloids Surf., A* **1996**, *107*, 57.

(26) Lacava, L. M.; Lacava, B. M.; Azevedo, R. B.; Lacava, Z. G. M.; Buske, N.; Tronconi, A. L.; Morais, P. C. Nanoparticle sizing, a comparative study using atomic force microscopy, transmission electron microscopy, and ferromagnetic resonance. *J. Magn. Magn. Mater.* **2001**, *225*, 79.

(27) Zeng, X.; Koshizaki, N.; Sasaki, T. A direct comparison of sizes characterized by TEM and AFM for Fe_2O_3 nanoparticles prepared by laser ablation. *Appl. Phys. A* **1999**, *69* (Suppl.), S253.

(28) Jolivet, J. P; Chanéac, C.; Tronc, E. Iron oxide chemistry. From molecular clusters to extended solid networks. *Chem. Commun.* **2004**, 481.

(29) JCPDS 33-0664.

(30) García, R.; Pérez. R. Dynamic atomic force microscopy methods. *Surf. Sci. Rep.* **2002**, *47*, 197.

(31) Hou, B.; Wu, Y.; Wu, L.; Shi, Y.; Zou, K.; Gai, H. Hydrothermal synthesis of cubic ferric oxide particles. *Mater. Lett.* **2006**, *60*, 3188.

(32) Yang, R.; Gao, L. Synthesis of single-crystal β-$Ni(OH)_2$ nanodisks and α-Fe_2O_3 nanocrystals in $C_2H_5OH-NaOH-NH_3{\cdot}H_2O$ system. *J. Colloid Interface Sci.* **2006**, *297*, 134.

(33) The crystallographic plane closest to the one containing the cross section is (−37 11 −60), making with the top face (−114) an angle of 90.08°. The third segment of the cross section is very close to the crystallographic axis [−3 28 7], the latter making with the [−4 −8 1] axis an angle of 63.9°.